Transition region-based approach for skin lesion segmentation

Priyadarsan Parida[*] and Ranjita Rout[+]

* *Department of Electronics and Communication Engineering, GIET University, Gunupur-765022, Rayagada, India*
\+ *Department of Electronics and Communication Engineering, GIET University, Gunupur-765022, Rayagada, India*

Abstract

Skin melanoma is a skin disease that affects nearly 40% of people globally. Manual detection of the area is a time-consuming process and requires expert knowledge. The application of computer vision techniques can simplify this. In this article, a novel unsupervised transition region-based approach for skin lesion segmentation for melanoma detection is proposed. The method starts with the Gaussian blurring of the green channel dermoscopic image. Further, the transition region is extracted using local variance features and a global thresholding operation. It achieves the region of interest (binary mask) using various morphological operations. Finally, the melanoma regions are segregated from normal skin regions using the binary mask. The proposed method is tested using the DermQuest dataset along with the ISIC 2017 dataset, and it achieves better results as compared to other state-of-the-art methods in effectively segmenting the melanoma regions from the normal skin regions.

Keywords: Skin melanoma, Transition region, Morphological operation, Gaussian blurring.

1   Introduction

Melanoma, generally referred to as skin cancer, affects 40% of the world's population. Its effect can be well understood from the statistics that the American Cancer Society has an estimated 96,480 number of new cases to be diagnosed in the year 2019. It also accounts for 75% of deaths associated with skin cancer. So, early screening is a crucial step for limiting the deaths caused due to it. Computer vision plays an important role in the early screening of melanoma. With the advent of the digital dermatoscope, the experts are able to visualize the filtered and magnified versions of the skin lesions that account for melanoma. The same images can be acquired digitally and processed using computer vision algorithms for early detection of the disease. A number of computer vision algorithms have been proposed for automatic detection of skin lesions, indicating whether it is malignant or benign.

Computer vision algorithms for early screening of skin melanoma have been utilized for the last two decades. Typically, the process is limited to the classification of melanoma until 2002 [1]. Further, the process of recognition, along with the accurate extraction of pigmented lesions using various image segmentation approaches, has been proposed by various researchers. The segmentation approaches developed for the said cause can be broadly categorized into 5 types as boundary-based, thresholding based [2], region-based, clustering approaches [3], and hybrid approaches. Hybrid approaches combine one or more approaches to provide better segmentation results. The active contour [4], graph cuts, saliency [5], and

transition region approaches are some hybrid approaches used in image segmentation. Apart from the above-mentioned approaches a number of supervised techniques utilizing different deep learning approaches have been proposed by different researchers for skin lesion segmentation [6]. Among them, the transition region-based approach is the simplest one using a combination of thresholding based and region-based approach.

Transition region-based approaches [7–9] developed so far are applicable only for photographic images containing single and multiple objects. Nevertheless, it has not been applied to skin melanoma images due to certain challenges like the strong appearance of background texture as compared to the Region of Interest (ROI), the overlapping of the intensity levels near the ROI boundary with the skin intensity levels, etc. Therefore, this paper intends to utilize the transition region-based approach for skin lesion segmentation by overcoming the above-mentioned challenges.

The rest of the paper is organized as: Section 2 describes the proposed skin lesion segmentation method. The various performance measures used for measuring the segmented lesions are given in Section 3. The results achieved, along with the discussion of the proposed method is given in Section 4. Finally, the article is concluded in Section 5.

2   Proposed Method

The proposed method begins with the extraction of the Green channel image from the macroscopic input image. It blurs the Green channel image using a Gaussian blurring filter. Further, the local variance features are extracted from the blurred image. It extracts transition regions from the local variance features using a global threshold. Further, using morphological operations, the segmentation mask of the ROI is obtained. Finally, via the segmentation mask, the required regions of interest are extracted from the Green channel. The detailed architecture of the proposed approach is given in Fig.1. Each step is discussed in detail in the subsections below:

Extraction of color components:

The dermoscopic images obtained by the dermatoscope are RGB images of human skin. The images constitute two regions: healthy skin regions and lesion regions. The lesion regions constitute a typical pigment network of black, brown, or gray color. Initially, the R, G, and B color components are separated from the RGB image, and the G-channel image is utilized for subsequent stages for processing. The G-channel provide maximum intensity components compared to R-channel and B-channel. Moreover, the human eye is more sensitive to brightness than chromaticity. So, the G-channel is preferred over other channels. The original images, along with different channels, are demonstrated in Fig.2. Fig.2 (c) shows the G-channel image (Green component) utilized for further processing.
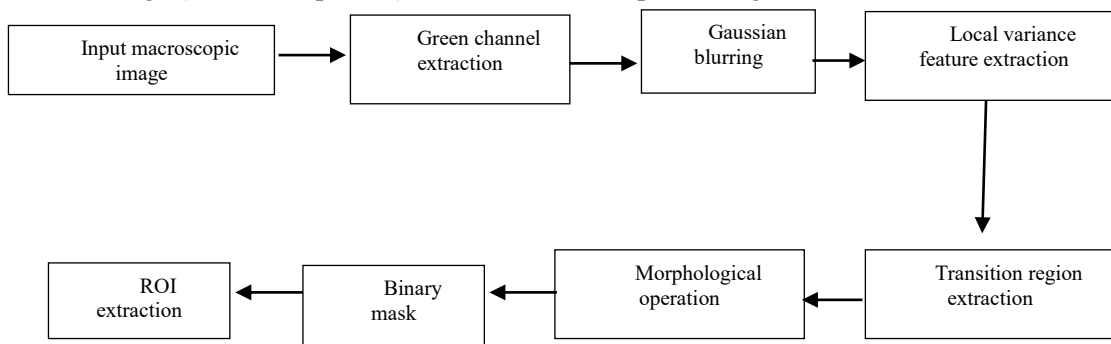

Fig.1. Architecture of the proposed method.

Blurring the Green channel image:

The G-channel extracted from the previous step has uneven illumination variation with sharp textures in the healthy skin regions as well as in lesion regions. The blurring phenomenon is strongly related to human visual perception. It allows the visual system to resolve the fine target details [10]. The same phenomenon is utilized in the proposed method to suppress the textures present in the image and smooth the image for identifying the target lesion regions in the textured healthy skin background. Here, a Gaussian blurring filter

is used with a standard deviation value σ of 5. It results in a blurred image of the G-channel image achieved from the former step. The effect of blurring of the G-channel image using a Gaussian blurring function with σ=5 is demonstrated in Fig.3(b).

Extraction of the local variance features:

The blurred G-channel image obtained from the previous step provides a smooth varying image with the lesion regions and healthy skin regions. The intended region of interest, i.e., the lesion regions, has darker intensity as compared to the healthy skin regions or the background. The pixels lying between the background and the region of interest (foreground) have a higher variance as compared to other pixels. Therefore, the proposed approach has explored the local variance features of the blurred G-channel image. The local variance is calculated in subsequent steps :

For a given local neighborhood of size $m \times m$ within an image, it gives the local variance as

$$lv(i, j) = \frac{1}{m^2 - 1} \sum_{x=1}^{m} \sum_{y=1}^{m} \left(p(x, y) - \bar{p}^2 \right), \tag{1}$$

where the local coordinate of the neighborhood of p is given by (x, y) and $\bar{p}$ is the mean of the neighborhood. It performs this operation throughout the image from left to right and top to bottom to achieve the local variance feature image given by

$$lv = \begin{bmatrix} lv(1,1) & lv(1,2) & ... & lv(1, N) \\ lv(2,1) & lv(2,2) & ... & lv(2, N) \\ ... & ... & ... & ... \\ lv(M,1) & lv(M,2) & ... & lv(M, N) \end{bmatrix}, \tag{2}$$

where, the size of the original image is given by $M \times N$. This results in a local variance feature image where the local variance features highlights the boundary regions between the background and the regions of interest. The local variance feature image extracted from the blurred image Fig. 3(b) is shown in Fig. 4(a).
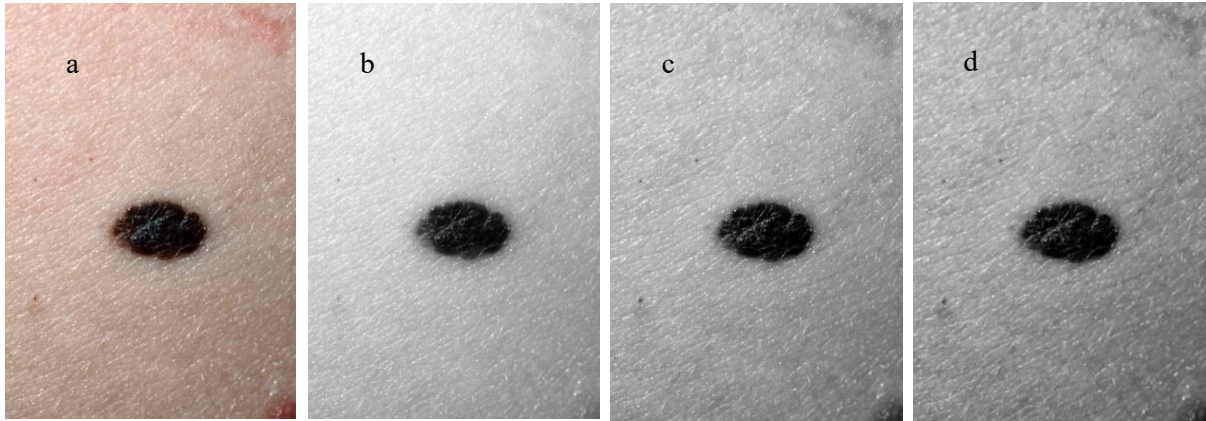

Fig. 2. (a) Original color image; (b) R-channel image; (c) G-channel image; (d) B-channel image.

Extraction of transition regions from the local variance features:

The local variance features achieved from the former sub-step contain the pixels separating the foreground regions (region of interest) from the background regions. These regions act as a boundary in separating two different regions. The boundary regions are effectively separated by applying thresholding operation on the local variance features. The method utilizes a global threshold value called the standard deviation of the feature matrix obtained from the former sub-step. It compares the local variance features with the threshold as

$$Tg(i, j) = \begin{cases} 1 & if \quad lv(i, j) \geq threshold \\ 0 & if \quad lv(i, j) < threshold \end{cases}, \tag{3}$$

where, the threshold is calculated as

$$threshold = \left(\frac{1}{M \times N} \sum_{x=1}^{M} \sum_{y=1}^{N} \left(lv(x, y) - E \right)^2 \right)^{\frac{1}{2}} \quad . \tag{4}$$

E is the expected or mean value given as

$$E = \frac{1}{M \times N} \sum_{x=1}^{M} \sum_{y=1}^{N} lv(x, y) \quad . \tag{5}$$

At the end of this process, a binary image is achieved where the transition regions are labelled as 1, and it labels the remaining regions as 0. It can be observed that the transition regions surround the region of interest. To show the result, the variance feature image resulted in Fig. 4 (a) is applied with the above-mentioned thresholding process to result in a thresholded image given in Fig. 4 (b). It can be well remarked that the transition regions extracted from the thresholding operation serve as a boundary between the skin lesions and the healthy skin regions.
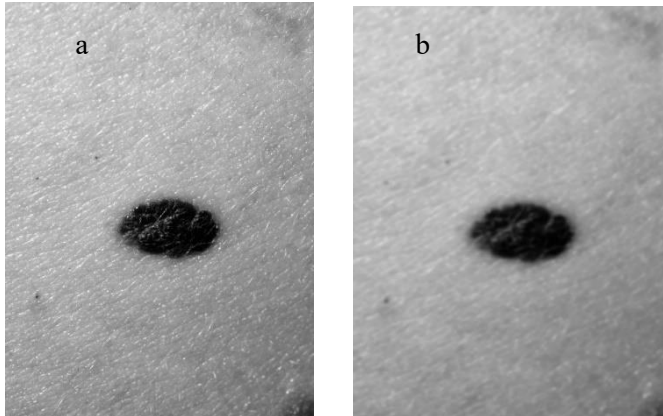

Fig.3. Effect of blurring on G-channel image: (a) G-channel image; (b) Blurred image (Gaussian blurring with $\sigma = 5$).

Morphological operations for segmentation mask extraction:

The transition regions obtained form the separating boundary between the background and foreground. So, in this step, it performs morphological operations using the transition regions obtained from the former step to extract the region of interest (foreground) from the binary images. The morphological region filling operation is applied considering the perimeter of the transition regions. The region filling operation results in a binary image containing two different regions, such as the region of interest (foreground regions) labeled as 1's and background regions (healthy skin regions) labeled as 0's. This is also referred to as the segmentation mask. The region filling operation discussed above is applied to the Fig. 4 (b) to get the segmentation mask shown in Fig. 4 (c).
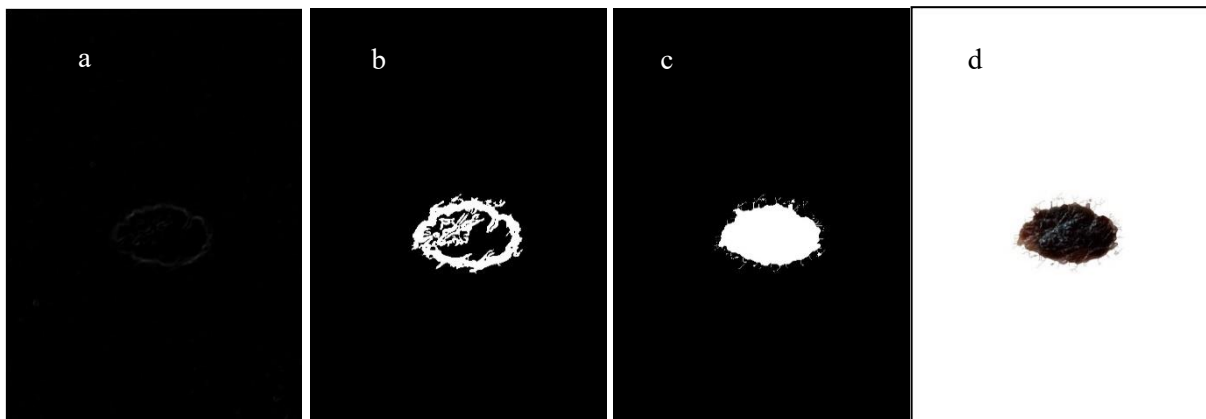

Fig. 4. (a) Local variance based features; (b) Thresholded image from (a); (c) Output of morphological region filling operation (segmentation mask); (d) Extracted skin lesion. region.

Extraction of skin lesion regions via segmentation mask:

The segmentation mask achieved from the former sub-step is a binary image with foreground regions labeled as 1's and background regions labeled as 0's. Using this mask, extract the modified R-channel, G-channel, and B-channel by replacing the regions with 1's with their corresponding intensities from the original R-channel, G-channel, and B-channel images. The 0's are replaced with a value of 255, indicating the background (healthy skin) regions. These modified images are combined to form the RGB image where their actual color components denote the skin lesion regions in the segmented image, and the background regions are made white indicating it as healthy skin regions. The results of the extraction of skin lesion from the segmentation mask shown in Fig. 4 (c) is given in Fig. 4 (d). Fig. 4 (d) shows the final skin lesion extracted from the original image shown in Fig. 2(a).
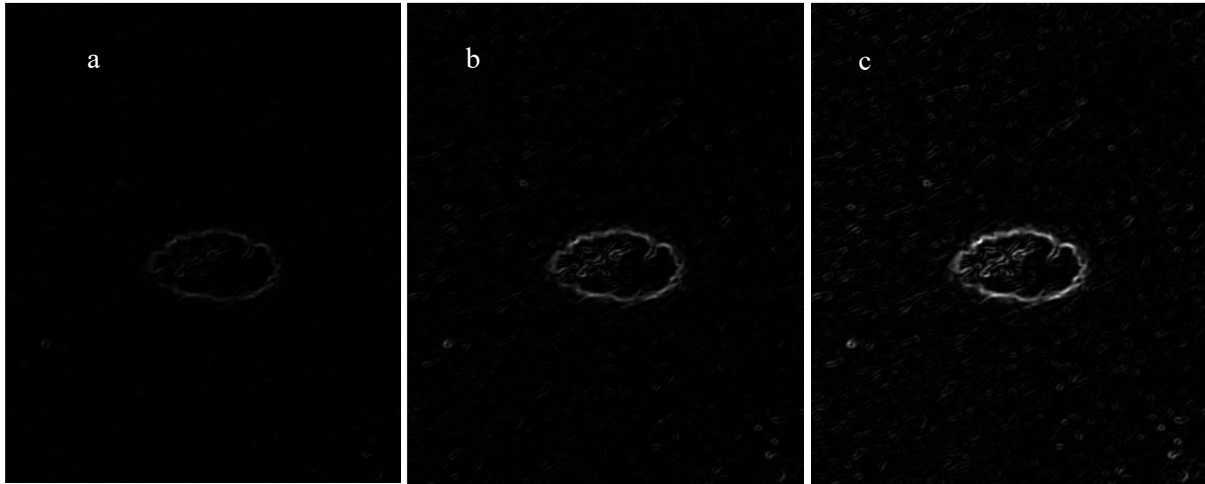

Fig. 5. Effect of window size for local variance feature extraction: (a) Feature image for 3×3 window; (b) Feature image for 5×5 window; (c) Feature image for 7×7 window.

3   Performance Analysis

The dermoscopic images used in experimentation are collected from the DermQuest dataset [11] and ISIC 2017 dataset [12]. The performance of the proposed approach is measured via 5 different metrics, such as Specificity, Sensitivity, Accuracy, and F-measure. For calculating the afore-mentioned performance measures, the segmentation mask generated by a particular method is compared with the ground truth image available in the dataset. Based on the comparison, a confusion matrix is created containing the true positives (TP), true negatives (TN), false positives (FP), and false negatives (FN) [13]. Based on these 4 basic parameters the other parameters such as Specificity, Sensitivity, Accuracy and F-measure are calculated.

Sensitivity:

The Sensitivity [14] is defined as the probability that the region is the actual skin lesion or not which is also called a true positive rate (TPR) given as

$$Sensitivity = \frac{TP}{TP + FN} \qquad . \tag{6}$$

The value ranges between 0 and 1, where the value 0 indicates the worst value, while the 1 indicates the best value.

Specificity:

The Specificity [14] reflects the negative values provided by the segmentation approach with respect to the actual negative values provided by the ground truth data which is defined as

$$Specificity = \frac{TN}{TN + FP} \qquad . \tag{7}$$

The Specificity value lies between 0 and 1, where 0 indicates the healthy regions are classified as lesions while 1 indicates healthy skin regions are classified as such.

Accuracy:

The Accuracy [15] is defined as the measure of the closeness of the proposed segmentation mask with the ground truth given by the experts. The Accuracy is given as

$$Accuracy = \frac{TP+TN}{TP+FP+TN+FN} \qquad . \tag{8}$$

The Accuracy takes a value between 0 and 1, where 0 indicates the worst segmentation result, and 1 corresponds to the best segmentation result.

Jaccard Index:

The Jaccard index (JI) [16] is a similarity measure that provides a comparison of the degree of the similarity and diversity between the segmented result with that of the ground truth. Mathematically, it is given as

$$JI = \frac{TP}{TP+FP+FN} \qquad . \tag{9}$$

The value of the Jaccard index lies between 0 and 1, where the higher value indicates better segmentation results.

Dice coefficient:

The Dice coefficient (DC) [16,17] is a similarity measure unlike the Jaccard coefficient, but the difference is it is a weighted one indicating the percentage of overlap between segmentation result and ground truth. Mathematically, it is given as

$$DC = \frac{2TP}{2TP+FP+FN} \, . \tag{10}$$

4   Results and Discussion

The experiment is carried out on a PC with a Core-i3 processor with 8G RAM in the MATLAB environment. The original images, along with their corresponding ground-truth images, are collected from the DermQuest dataset [11] and ISIC 2017 dataset [12]. The proposed work is carried out for the extraction of melanoma skin lesions from healthy skin regions.

The major parameter that plays an important role in this work is the local variance feature extraction. For it, the proposed method utilizes the window size of 3×3. To validate it, experimentation was performed with a higher-order window size. It can be observed from Fig.5 that increasing the local window size enhances the local variance more prominently. But careful observation of Fig. 5 (a) indicates that a smaller window size of 3×3 only highlights the regions having a higher variance, i.e., near the regions where there is a high transition between the pixel intensities. But when the window size increases, i.e., in Fig. 5 (b) and Fig. 5 (c), it tries to intensify the regions where the variance is comparatively low, indicating the false transitional regions. The transition regions are extracted from these high variance regions. Therefore, it has been considered the local window size to be 3×3 instead of a higher-order window size.

The proposed method is tested with a wide variety of images available in the Dermaquest dataset and ISIC 2017 dataset [12], and it is observed that it accurately segments the skin lesion portions from the healthy skin regions. The qualitative measures can be seen from the segmentation results of some images are shown in Fig.6. The quantitative evaluation of the segmentation results is provided in terms of different performance measures such as Accuracy, Dice coefficient, Jaccard index, Specificity, and Sensitivity for two different datasets given in Table1 and Table 2. The proposed method is compared with the different state of art approaches for skin lesion segmentation such as star shape prior in the fully convolutional network (SSP) [18], deeply supervised rotation-equivariant network (DSREN) [19], deep residual architecture [20], and efficient skin lesion segmentation using a separable-Unet with stochastic weight averaging (SU-SWA) [6]. The proposed method achieved good segmentation results in the skin lesion segmentation utilizing the ISIC 2017 image dataset. The comparisons are shown in Table 1 that compares the proposed approach with traditional segmentation approaches along with recent machine learning approaches. Similarly, four different

recent state-of-the-art techniques performing skin lesion segmentation like automated skin lesion segmentation using cellular automata (ASLCA) [21], segmentation of skin lesions using joint statistical texture distinctiveness (SLSJSTD) [22], multi-scale contrast based skin lesion segmentation (MCSLS) [23], and simple weighted thresholding method for segmentation of pigmented skin lesions (SWOT) [24] using the DermQuest dataset are compared with the performance of the proposed method. The quantitative performance measures for different methods, along with the proposed approach is given in Table 2.

Method	Accuracy	DC	JI	Sensitivity	Specificity
SSP [18]	93.8	85.7	77.3	85.5	98.5
DSREN [19]	93.55	85.60	77.23	85.40	97.59
DRASLS [20]	93.6	85.6	76.5	83	98.5
SU-SWA [6]	94.31	86.93	79.26	**89.53**	96.32
Proposed Method	**96.8**	**90.6**	**83.2**	83.9	**99.8**

Table 1: Comparison of Skin Lesion Segmentation on the ISIC 2017 dataset.

Method	Accuracy	DC	JI	Sensitivity	Specificity
ASLCA [21]	**98.80**	--------	-------	93.08	**99.08**
SLSJSTD [22]	97.6	--------	--------	90.8	99.5
MCSLS [23]	98.21	-------	-------	87.89	99.45
SWOT [24]	96.5	-------	-------	87.23	97.78
Proposed Method	98.4	80.2	68.7	**95.5**	98.5

Table 2: Comparison of Skin Lesion Segmentation on the DermQuest dataset.

The qualitative results can be visualized from Fig. 6. Here, it can be observed that the proposed method effectively segments the lesion regions given in Fig. 6 (b) from the original dermoscopy images given in Fig. 6 (a). The same can also be verified when the ground-truth images in Fig. 6 (c) are compared with the segmentation mask of the proposed method shown in Fig. 6 (d). It can also be observed from Fig. 6 (c) and Fig. 6(d) that the segmentation mask exhibit a high degree of similarity with respect to the ground-truth images with a very less emergence of background healthy skin regions and accurately segregates the lesion regions with less loss of foreground (lesion) regions. Similarly, quantitative performance values given in Table 1 and Table 2 indicate that the proposed approach outperforms all existing approaches, thereby providing better segmentation results. The best values for all performance measures of different methods are marked as bold. For the ISIC 2017 dataset, the proposed approach provides the best performances except in terms of the Sensitivity. For the ISIC 2017 dataset, the method SU-SWA [6] attains the best sensitivity value. For the DermQuest dataset, the proposed method attains an accuracy level of 98.4, which is almost nearly equal to the best value provided by the method ASLCA given in Table 2. The same is in case of Specificity, where the average Specificity of the proposed approach is 98.5 that is almost nearly equal to that of the method ASLCA. For the DermQuest dataset, the proposed approach provides the best sensitivity value given in Table 2.

From both the tables (Table 1 and Table 2) indicating quantitative measures, it is evident that the proposed method being a simpler approach outperforms the existing skin lesion segmentation approaches. The same can be verified qualitatively (visual inspection) from the segmentation results given in Fig.6.
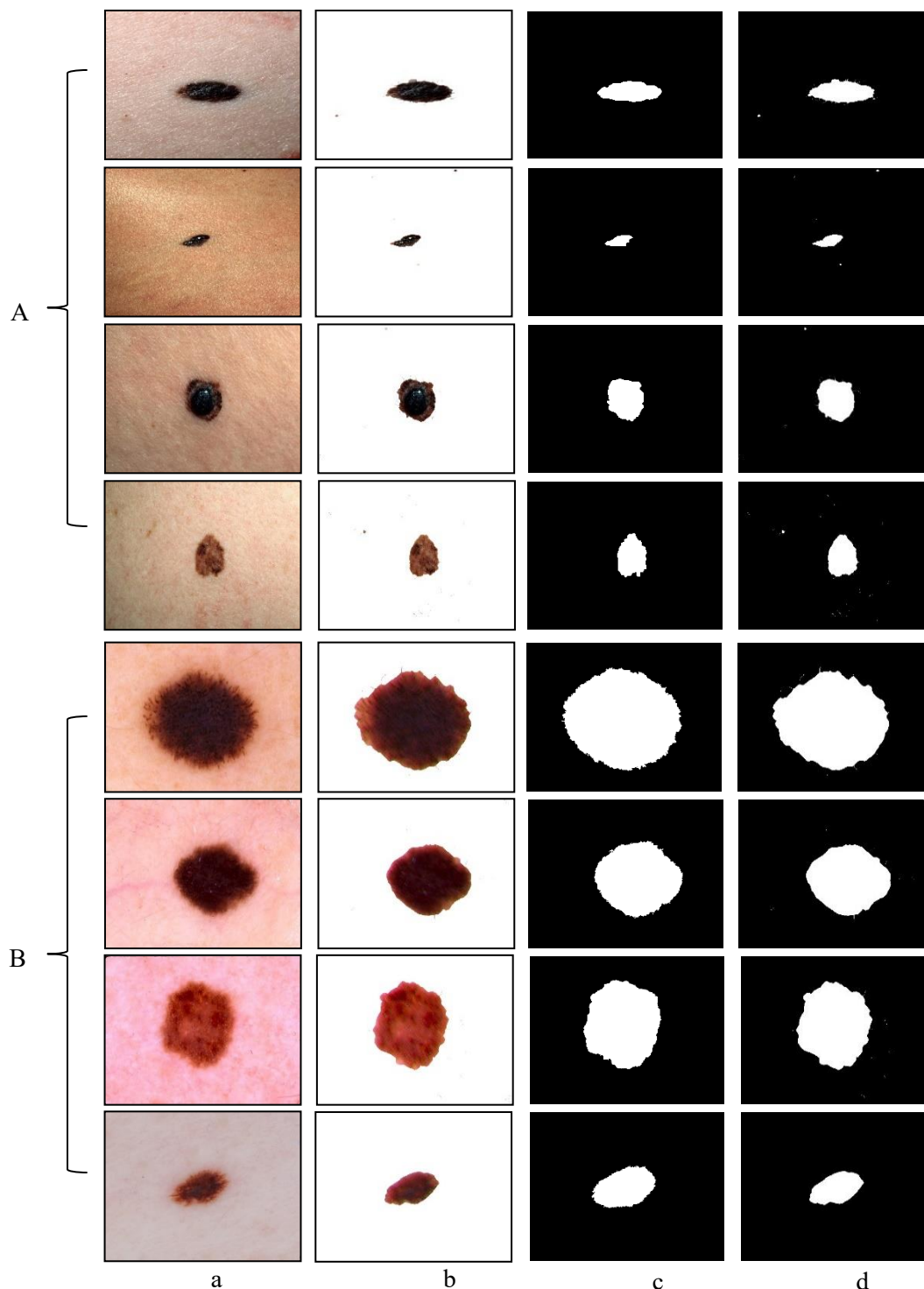
Fig. 6. Original images, ground truth, segmentation results and segmentation mask of different datasets. (A) DermQuest dataset; (B) ISIC 2017 dataset: (a) Original RGB image; (b) corresponding segmentation result of the proposed method; (c) ground truth; (d) segmentation mask of the proposed method.

5   Conclusion

The paper presents a novel approach to skin lesions segmentation of skin melanoma dermoscopic images. The approach utilizes local variance along with a global threshold for skin lesion segmentation. Experimental results reveal that the proposed approach provides better lesion segmentation of dermoscopic images with

better accuracy as compared to the existing state of art approaches developed for skin lesion segmentation. Visual perception of the results indicates that the boundaries, along with lesion regions and the background (healthy skin regions) are well separated and differentiable.

References

[1]   G. Joel, P. Schmid-Saugeon, D. Guggisberg, et al., "Validation of segmentation techniques for digital dermoscopy", *Skin research and technology : official journal of International Society for Bioengineering and the Skin (ISBS) [and] International Society for Digital Imaging of Skin (ISDIS) [and] International Society for Skin Imaging (ISSI)*, 8(4):240–249, 2002. DOI: 10.1034/j.1600-0846.2002.00334.x

[2] R. Kaur, R. LeAnder, N.K. Mishra, et al., "Thresholding methods for lesion segmentation of basal cell carcinoma in dermoscopy images", *Skin research and technology : official journal of International Society for Bioengineering and the Skin (ISBS) [and] International Society for Digital Imaging of Skin (ISDIS) [and] International Society for Skin Imaging (ISSI)*, 23(3):416–428, 2017. DOI: 10.1111/srt.12352

[3] N. Nida, A. Irtaza, A. Javed, M.H. Yousaf, M.T. Mahmood, "Melanoma lesion detection and segmentation using deep region based convolutional neural network and fuzzy C-means clustering", *International journal of medical informatics,* 124:37–48, 2019. DOI: 10.1016/j.ijmedinf.2019.01.005

[4] F. Riaz, S. Naeem, R. Nawaz, M.T. Coimbra, "Active Contours Based Segmentation and Lesion Periphery Analysis For Characterization of Skin Lesions in Dermoscopy Images", *IEEE journal of biomedical and health informatics,* 23(2):489–500, 2019. DOI: 10.1109/JBHI.2018.2832455

[5] M.A. Khan, T. Akram, M. Sharif, et al., "Construction of saliency map and hybrid set of features for efficient segmentation and classification of skin lesion", *Microscopy research and technique*, 82(6):741–763, 2019. DOI: 10.1002/jemt.23220

[6] P. Tang, Q. Liang, X. Yan, et al., "Efficient skin lesion segmentation using separable-Unet with stochastic weight averaging", *Computer Methods and Programs in Biomedicine,* 178:289–301, 2019. DOI: 10.1016/j.cmpb.2019.07.005

[7] P. Parida, N. Bhoi, "Wavelet based transition region extraction for image segmentation", *Future Computing and Informatics Journal,* 2(2):65–78, 2017. DOI: 10.1016/j.fcij.2017.10.005

[8] P. Parida, N. Bhoi, P. Dewangan, "Colour image segmentation based on transition region and morphological operation", *IEEE Proc. of 2017 International Conference on Wireless Communications, Signal Processing and Networking,* 62:1293–1297, 2017. DOI: 10.1109/WiSPNET.2017.8299972

[9] Z. Li, K. Tang, Y. Cheng, Y. Hu, "Transition region-based single-object image segmentation", *AEU - International Journal of Electronics and Communications*, 68(12):1214–1223, 2014. DOI: 10.1016/j.aeue.2014.06.010

[10] G. Maiello, L. Walker, P.J. Bex, F.A. Vera-Diaz, "Blur perception throughout the visual field in myopia and emmetropia", *Journal of Vision,* 17(5):1-13, 2017. DOI: 10.1167/17.5.3

[11] R. Amelard, J. Glaister, A. Wong, D.A. Clausi, "High-Level Intuitive Features (HLIFs) for Intuitive Skin Lesion Description", *IEEE Transactions on Biomedical Engineering,* 62(3):820–831, 2015. DOI: 10.1109/TBME.2014.2365518

[12] N.C.F. Codella, D. Gutman, M.E. Celebi, et al., "Skin lesion analysis toward melanoma detection: A challenge at the 2017 International symposium on biomedical imaging (ISBI), hosted by the international skin imaging collaboration (ISIC)", *Proc. of International Symposium on Biomedical Imaging,* 2018:168–172, 2018. DOI: 10.1109/ISBI.2018.8363547

[13] K. Møllersen, M. Zortea, T.R. Schopf, H. Kirchesch, F. Godtliebsen, "Comparison of computer systems and ranking criteria for automatic melanoma detection in dermoscopic images", *Plos One,* 12(12):1-11, 2017. DOI: 10.1371/journal.pone.0190112

[14] J. Jaworek-Korjakowska, P. Kleczek, "eSkin: Study on the Smartphone Application for Early Detection of Malignant Melanoma", *Wireless Communications and Mobile Computing,* 2018:1–11, 2018. DOI: 10.1155/2018/5767360

[15] F.F. Ximenes Vasconcelos, A.G. Medeiros, S.A. Peixoto, P.P. Rebouças Filho, "Automatic skin lesions segmentation based on a new morphological approach via geodesic active contour", *Cognitive Systems Research*, 55:44–59, 2019. DOI: 10.1016/j.cogsys.2018.12.008

[16] H.R. Tizhoosh, A.A. Othman, "Anatomy-aware measurement of segmentation accuracy", *SPIE 9784 Proc. of Conf. On Medical Imaging 2016: Image Processing*, California, 1:301–310, 2016. DOI: 10.1117/12.2214869

[17] W.R. Crum, O. Camara, D.L.G. Hill, "Generalized overlap measures for evaluation and validation in medical image analysis", *IEEE transactions on medical imaging*, 25(11):1451–61, 2006. DOI:

10.1109/TMI.2006.880587

[18] Z. Mirikharaji, G. Hamarneh, "Star Shape Prior in Fully Convolutional Networks for Skin Lesion Segmentation", *Lecture Notes in Computer Science (including subseries Lecture Notes in Artificial Intelligence and Lecture Notes in Bioinformatics)*, 11073:737–745, 2018. DOI: 10.1007/978-3-030-00937-3_84

[19] X. Li, L. Yu, C.W. Fu, P.A. Heng, "Deeply supervised rotation equivariant network for lesion segmentation in dermoscopy images", *Lecture Notes in Computer Science (including subseries Lecture Notes in Artificial Intelligence and Lecture Notes in Bioinformatics)*, 11041:235–243, 2018. DOI: 10.1007/978-3-030-01201-4_25

[20] G.M. Venkatesh, Y.G. Naresh, S. Little, N.E. O'Connor, "A deep residual architecture for skin lesion segmentation", *Lecture Notes in Computer Science (including subseries Lecture Notes in Artificial Intelligence and Lecture Notes in Bioinformatics)*, 11041:277–284, 2018. DOI: 10.1007/978-3-030-01201-4_30

[21] L. Bi, J. Kim, E. Ahn, D. Feng, M. Fulham, "Automated skin lesion segmentation via image-wise supervised learning and multi-scale superpixel based cellular automata", *IEEE Proc. of 13th International Symposium on Biomedical Imaging (ISBI)*, Prague, 22:1059–1062, 2016. DOI: 10.1109/ISBI.2016.7493448

[22] J. Glaister, A. Wong, D.A. Clausi, "Segmentation of Skin Lesions From Digital Images Using Joint Statistical Texture Distinctiveness", *IEEE Transactions on Biomedical Engineering,* 61(4):1220–1230, 2014. DOI: 10.1109/TBME.2013.2297622

[23] I. Filali, M. Belkadi, "Multi-scale contrast based skin lesion segmentation in digital images", *Optik,* 185:794–811, 2019. DOI: 10.1016/j.ijleo.2019.04.022

[24] M. Zortea, E. Flores, J. Scharcanski, "A simple weighted thresholding method for the segmentation of pigmented skin lesions in macroscopic images", *Pattern Recognition,* 64:92–104, 2017. DOI: 10.1016/j.patcog.2016.10.031